Ultrafast Electron Dynamics at Ice−Metal Interfaces: Competition between Heterogeneous Electron Transfer and Solvation

Julia Stähler,* Cornelius Gahl, Uwe Bovensiepen, and Martin Wolf

Fachbereich Physik, Freie Universität Berlin, Arnimallee 14, 14195 Berlin-Dahlem, Germany

Received: January 25, 2006

Microscopic insight into heterogeneous electron transfer requires an understanding of the participating donor and acceptor states and of their respective interaction. In the regime of strong electronic coupling, two limits have been discussed where either the states overlap directly or the states are separated by a potential barrier. In both situations, the transfer probability is determined by the magnitude of the wave function overlap, whereby in the case of the potential barrier, its width and height are rate limiting. In our study, we observe a dynamical crossover between these two regimes by investigating the electron-transfer dynamics of localized, solvated electrons at ice−metal interfaces. Employing femtosecond time-resolved two-photon photoelectron spectroscopy, we analyze the population dynamics of excess electrons in the ice layer, which experience the competing processes of transfer to the metal electrode and energetic stabilization in the ice by molecular reorientation. Comparing the dynamics of D_2O on Cu(111) and Ru(001), we observe an early regime at $t <$ 300 fs, where the transfer time is determined by wave-function overlap with the metal and a second regime ($t >$ 300 fs), where the transfer proceeds nearly independent of the substrate. The assignment of these two regimes to the established mechanisms of electron transfer is backed by an empirical model calculation that reproduces the experimental data in an excellent manner.

Introduction

Heterogeneous electron transfer at solid−molecular interfaces is of fundamental importance and technological relevance in seemingly different areas ranging from classical electrochemistry, surface photochemistry, dye-sensitized solar cells, and nanoscale electronic devices.[1,2] For example, in the emerging field of molecular electronics, the key issue is charge transport through metal−molecule−metal junctions, which comprises interfacial electron transfer across both metal−molecule contacts.[3,4] An understanding of such charge transfer requires knowledge about the electronic coupling strength between the metal electrode with delocalized Bloch states exhibiting periodic wave functions and the states in the molecular environment where the electrons tend to localize by polaron or exciton formation.[5] Such localization phenomena are induced by the excess charge and are mediated by molecular reorganization which is also fundamental for understanding solvation processes in polar media. In particular, the electron solvation in water has always been in the focus of research due to its fundamental importance as a model system for solvation phenomena.[6−8] Recently, a number of studies have focused on electron solvation in water-anion clusters. However, details about formation, structure, and relaxation dynamics are still under debate.[9−11]

Here we use a new ansatz to obtain insight into the mechanisms of heterogeneous electron transfer by a combined investigation of electron solvation and interfacial charge transfer at the water−metal interface. We show that photoinduced electron injection into ultrathin ice films at metal surfaces provides an excellent model system to study the dynamics of charge transfer from the substrate into a molecular adlayer, the stabilization of electrons within the polar solvent, and the competing process of back relaxation to the metal. In previous investigations we have studied the dynamics and basic mechanisms of electron injection, localization, and solvation in water at the noble metal surface Cu(111).[12−15] In the present contribution, we disentangle the solvation and the transfer process by employing different metal substrates. By comparing Cu(111) and Ru(001), with their different electronic band structures and different water−metal interactions, a detailed understanding of the influence of both the intrinsic properties (electronic and structural) of the ice layers and the adsorbate−substrate interaction is achieved. In particular, we can discriminate between two established mechanisms of electron transfer at the adsorbate−metal interface mediated either by tunneling through a barrier or by direct coupling to the electronic states of the metal. These two regimes are illustrated in Figure 1. In panel (a), a stationary unoccupied state at a metal−molecule interface, which originates from the image potential in front of the metal and which is fully periodic within the interface plane (i.e., parallel to the interface), is considered. In a dielectric continuum description, a molecular adlayer would modify this image potential because the dielectric constant differs from unity, which affects binding energies and relaxation rates.[16,17] Relaxation of the electron in the image potential state (IPS) proceeds by electron transfer to metal bulk where it decays by electron−hole generation to the Fermi level E_F.[18] Because in this case the electronic structure of the metal determines transfer and decay probabilities, we term this electron-transfer regime the *substrate-dominated limit*. Note that the term *substrate* is used throughout the manuscript for the metal electrode. In general, this electrode can be a metal or a semiconductor, as in the case of the solid TiO_2 electrode in a Graetzel cell.[2]

* Corresponding author. E-mail: julia.staehler@physik.fu-berlin.de. Phone: +49-(0)30-838 53340. Fax: +49-(0)30-838 56059. Electronic address: www.physik.fu-berlin.de/∼femtoweb.

10.1021/jp060538c CCC: $33.50
Published on Web 04/27/2006

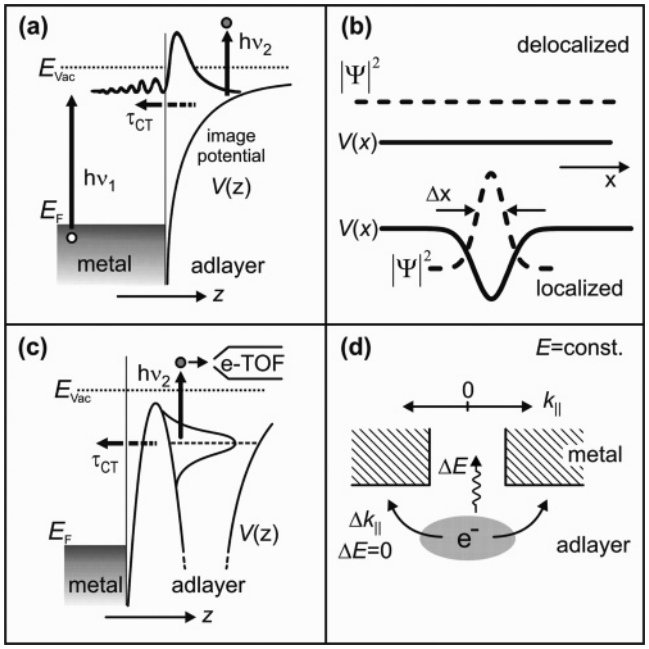

Figure 1. Left panels illustrate two limits of electron transfer at adsorbate−metal interfaces: (a) The charge-transfer time τ_{CT} of an electronic state that arises from an adsorbate-modified image potential is dominated by direct coupling to the metal states. $V(z)$ is the image potential in front of the metal. (c) For a negative ion resonance in front of a metal electrode, the back transfer probability $1/\tau_{CT}$ is determined by tunneling through the potential barrier with height ΔE. (b) Illustration of the spatial variation of the potential $V(x)$ and the electron's probability density $|\Psi|^2$ for a delocalized and a localized electronic state. The direction x is parallel to the surface. (d) Elastic and inelastic relaxation processes of an electron localized in the unoccupied resonance in the adlayer near the interface. At constant energy E, the electronic structure at the metal surface exhibits in many systems an orientational band gap, e.g., around the center of the surface Brillouin zone ($k_{||} = 0$). Hatched areas represent electronic states available for elastic scattering. Thus, elastic electron transfer is hindered at $k_{||} = 0$. States at larger $k_{||}$ are available if the electronic momentum parallel to the interface is changed by $\Delta k_{||}$.

Because the image potential varies with the direction z normal to the interface plane and the penetration of the electron into the bulk is hindered by an orientational band gap, IPS are localized along z near the interface. Within the interface plane, electrons in IPS form plane waves as a result of the constant potential along the lateral dimensions denoted as x (Figure 1b). The description of the molecular adlayer as a dielectric continuum disregards any spatial variation of the potential in the molecular environment. However, corrugation of the potential in the lateral direction may change the character of the electronic state from a plane wave toward a localized state. Moreover, a local dynamical response of the nuclei relevant for solvation processes is not included in a continuum approach. Idealized situations for localized and delocalized states are illustrated in Figure 1b. Because the interaction of the electronic states of the metal electrode and the molecular adlayer determine the electron-transfer probability, a realistic description must include the spatial variation of the potential in the molecular environment in both x and z directions. Figure 1c illustrates the case of an electron-transfer process between the metal and a molecular resonance like the lowest unoccupied molecular orbital (LUMO) of an adsorbate, for example, Cs/Cu(111).[19] For this case, a mechanism for electron transfer has been invoked where the transfer rate is determined by the tunneling probability through a potential barrier.[20] In the molecular environment of a solvent, a potential barrier can be formed that confines an excess electron in all three spatial dimensions, as is the case for solvated electrons. Here the potential barrier screens the electron by the rearrangement of the molecular dipoles from the metal. For sufficient well screening, the transfer process is governed solely by the potential barrier and the orbital character of the electronic state in the solvent (Figure 1c). Therefore, we refer to this limit of electron transfer as the *barrier-determined coupling* regime.

In our study, we analyze the mechanism of electron transfer for a localized electron in an ice adlayer, which changes its degree of confinement, Δx, dynamically during electron solvation. As will be shown below, this approach facilitates the observation of the crossover between the substrate-dominated and the barrier-determined regimes of electron transfer. This crossover is accompanied by the formation and the dynamical evolution of a potential barrier around the solvated electron at the interface. We show that this crossover is basically independent of the electronic band structure of the metal. As a consequence, the electron-transfer rates become time- and energy-dependent. Employing a simple empirical model calculation, we observe that this change of transfer rates affects the dynamical evolution of the solvated electron peak position in the photoelectron spectrum. Moreover, this model facilitates separation of the competing elementary processes of energetic stabilization of the solvated electron and transfer back to the metal substrate.

Note that the localization of the wave function to a spatial width Δx is described in terms of an electronic wave packet, which represents a nonstationary state and is formed by the superposition of plane waves within a momentum interval, Δp, according to the Heisenberg uncertainty relation. Relaxation of the excited LUMO state proceeds by electron transfer to the metal and is described by the spreading of the electron wave packet by tunneling through the potential barrier.

To follow arguments given below it is helpful to consider the elastic or inelastic character of the electron-transfer process. Single-crystal metal surfaces as employed in the experiment as metal electrodes are characterized by the surface electronic structure with orientational band gaps around the surface Brillouin zone center at an electron momentum component in the interface plane $k_{||} = 0$. Such a band gap at the energy of the resonance of the molecular state or the solvated electron inhibits an elastic transfer process along the normal direction, as depicted in Figure 1d. In the normal direction, that is, along $k_{||} = 0$, electron transfer is possible only for inelastic processes where a lower lying electronic state is available and the energy ΔE is dissipated to electron−hole pair excitations in the metal.[19] Elastic transfer (i.e., $\Delta E = 0$) from the resonance to the metal substrate, as depicted in Figure 1d, is possible if the electron momentum is changed by $\Delta k_{||}$, as has been investigated in detail earlier for Cs adsorbed on different single-crystal Cu surfaces.[19]

Experimental Details

The experimental setup combines an ultrahigh vacuum (UHV) chamber (base pressure $< 10^{-10}$ mbar) for in situ investigation of the ice−metal interfaces and a tunable amplified fs-laser system. Ultrathin D_2O layers were deposited via a pinhole doser under UHV conditions at $T \leq 100$ K onto Ru(001) and Cu(111) surfaces, which were prepared before adsorption by cycles of Ar^+ sputtering and annealing, as described previously.[15,21,22] The ice adlayers have been characterized by thermal desorption (TD) spectroscopy. In agreement with literature,[23,24] the TD spectra of D_2O/Ru(001) (shown in refs 14 and 25) exhibit two maxima. The peak at the higher temperature (178 K) saturates with

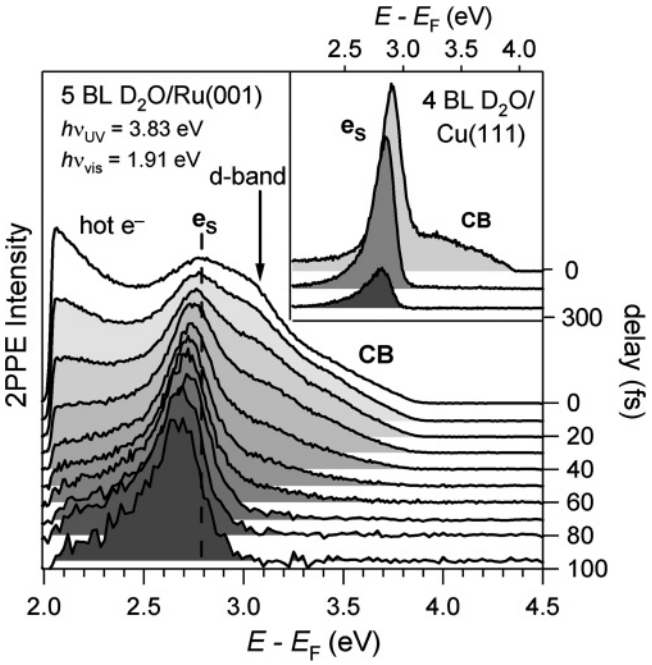

Figure 2. Time-resolved 2PPE spectra of amorphous D_2O layers on Ru(001) (main figure) and Cu(111) (inset) for different pump−probe delays. The intermediate state energy is given by the horizontal axes, time delay by the vertical offset (right axes). The D_2O/Ru(001) spectra are normalized to the peak maximum termed e_S.

increasing coverage and is attributed to desorption of the first bilayer (BL), while the second peak represents sublimation of further layers. The area under the TD spectrum of the first BL peak on Ru(001) is normalized to unity, allowing determination of the ice coverage on both substrates in units of BL. It is well-known that at temperatures $T < 100$ K amorphous ice layers are formed.[26] On Cu(111), only the sublimation process is observed as a result of the weaker bonding of D_2O on Cu.[27] While on Cu(111) the D_2O wets the metal for a coverage above 2−3 BL,[28] on Ru(001) an ordered first BL, whose exact appearance is still under debate,[29−32] is formed and further growth proceeds layerwise. Thus, we anticipate that the bulk of amorphous ice films on both substrates are comparable to each other, but the interface to the metal might be modified.

Time-resolved two-photon photoemission (2PPE) studies were performed with a commercial amplified Ti:sapphire laser system generating 800 nm laser pulses with 4 μJ of energy per pulse at a repetition rate of 200 kHz. This output drives two optical parametric amplifiers that generate tunable infrared (IR−OPA) and visible (VIS−OPA) femtosecond laser pulses with durations of 30 and 55 fs, respectively. As shown in Figure 1a, UV pump pulses $h\nu_1$, generated by frequency quadrupling/doubling, excite electrons to unoccupied, bound states above the Fermi level E_F. Time-delayed visible probe pulses, $h\nu_2 = h\nu_1/2$, photoemit the transient electron population in the intermediate state by exciting them to continuum states above the vacuum level, E_{vac}. The kinetic energy of these photoelectrons is determined for different delays between pump and probe pulses by an electron time-of-flight spectrometer. Because the dynamics in D_2O/Ru(001) proceed faster than in ice layers on Cu(111), the IR−OPA, which delivers shorter laser pulses compared to the output of the VIS−OPA, has been employed for the Ru system.

Experimental Results

Figure 2 shows representative 2PPE spectra of amorphous multilayers of D_2O on Ru(001) (main figure) and Cu(111) (inset) for a series of different time delays (right axes). The spectra are plotted as a function of intermediate state energy $E - E_F = E_{kin} + \Phi - h\nu_2$, where $\Phi = E_{vac} - E_F$ denotes the work function. Time-dependent 2PPE spectra of amorphous ice on Cu(111), shown in the inset, exhibit two adsorbate induced electronic states: (i) an energetically broad, short-lived continuum above $E - E_F = 3$ eV, which we previously identified to be the ice conduction band (CB) and (ii) a distinct peak at 2.9 eV above E_F, which we attributed to solvated electrons (e_S).[12,13] The peak maximum shifts to lower energies with increasing time delay as a result of an energetic stabilization of the solvated electrons caused by a rearrangement of the surrounding water molecules, that is, formation of the solvation shell. In addition, as will be demonstrated in this article, an energy-dependent electron transfer rate has to be taken into account. This leads to the conclusion that a shift of the observed solvated electron peak does not necessarily indicate a change in the binding energy. This finding emphasizes that, for microscopic insight, the competition between electron transfer and solvation dynamics is of central importance.

Corresponding features are also observed for D_2O/Ru(001).[33] To emphasize the dynamic evolution of the solvated electron peak e_S, the spectra in the main figure are normalized to their peak maxima. As observed for D_2O/Cu(111), the binding energy increases with time delay leading to a peak shift toward E_F. Two further spectral features are generated by the Ru substrate. These are hot electrons at the low-energy cutoff and a peak resulting from a surface resonance 1 eV above E_F arising from the unoccupied ruthenium $4d_{z^2}$-band.[34] In contrast to the solvated electron peak, these electrons near E_F are excited by visible light and probed by UV photons. Thus, their decay is monitored for the reversed pulse sequence, that is, at negative delays. The decay of adsorbate and substrate induced spectral contributions toward positive and negative delays, respectively, facilitates the assignment of the 2PPE features given in Figure 2, and we can safely concentrate on the dynamics of the solvated electrons in the ice layers. Note that for delays >50 fs, where no substrate-induced signal is found, the peak shape of e_S is comparable to the measurements on D_2O/Cu(111) given in the inset. Because the line shape of e_S has previously been attributed to an inhomogeneous distribution of solvation sites,[13] it is termed *solvated electron distribution* in the following.

On the basis of these observations, we conclude that the processes of electron solvation in amorphous multilayers of D_2O/Ru(001) are qualitatively the same as those in D_2O/Cu(111). However, we also find interesting quantitative differences. Figure 3 shows the energetic shift of the peak maximum of e_S for D_2O on Cu(111) (diamonds) and on Ru(001) (circles). In the latter case, the maximum approaches E_F with a rate $\Sigma_S^{Ru} = -0.83$ eV/ps, which is determined by a linear fit to the data indicated by the dashed line. In the case of D_2O/Cu(111), the maximum shifts three times slower with a rate $\Sigma_S^{Cu} = -0.27$ eV/ps. Note that the maxima of the solvated electron distribution on Ru(001) always lies below the corresponding value observed for Cu(111).[35] The decay of the solvated electron contribution occurs in parallel to the increase in binding energy. This observation brings up the question of whether the dynamical peak shift results from pure molecular reorientation or from electron transfer (i.e., decay back to the substrate) with an energy-dependent probability.

To study the population dynamics, we evaluate the temporal evolution of the 2PPE intensity for the solvated electron peak as a function of delay time t, which is referred to as a cross correlation (XC) trace. When an exponential decay of the

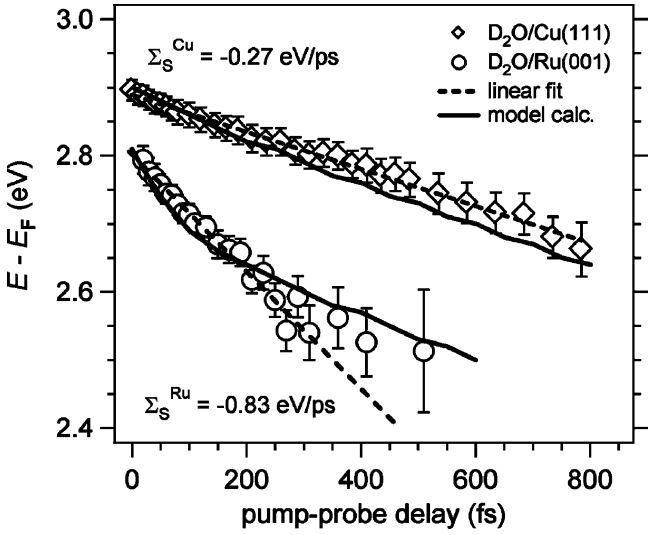

Figure 3. Time-dependent shift of the peak maximum e_S for D_2O on Cu(111) and Ru(001). The dotted lines are linear fits to the data and represent the shift of the peak maximum with delay $\Sigma_S(t)$; the peak maximum according to the model calculations is depicted by the solid lines.

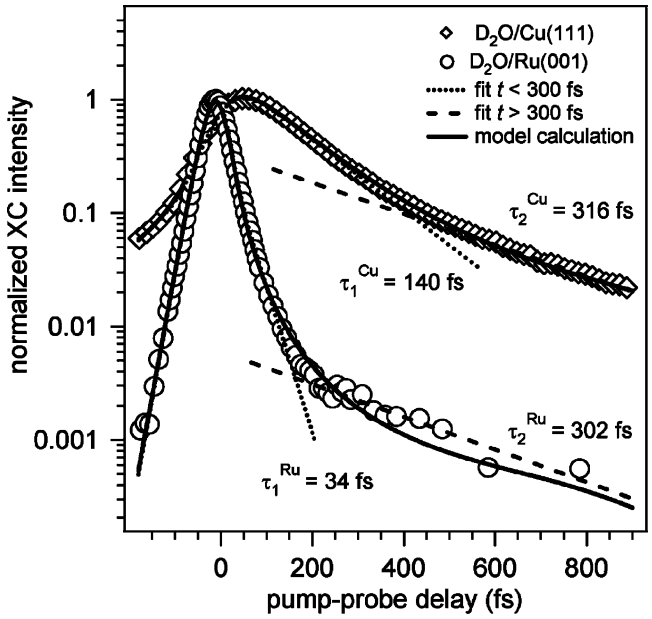

Figure 4. Cross-correlation traces of 2PPE intensity integrated over the e_S distribution for D_2O on Ru(001) (circles) and on Cu(111) on a logarithmic intensity axis. In the first case, data for 5 BL coverage are given. For D_2O/Cu(111) (squares) experimental results for 3−5 BL preparations have been averaged. This is possible because the solvation dynamics do not exhibit a coverage dependence for $\theta > 3$ BL.[15] The lines represent fits for early and late delay regimes and model calculations. For details, see the text.

electron population is considered, a transfer time is determined. To include the change in binding energy, the XC trace is integrated over the full energy window of the peak that is for D_2O/Ru(001), 2.4−2.8 eV and 2.4−2.9 eV in the case of D_2O/Cu(111). Both XC traces are given in Figure 4. The position of the maximum in the XC trace for D_2O/Cu at a positive delay time arises from the exponentially decaying population convoluted with the envelope of the laser pulse.[36] For D_2O/Ru(001), a significant contribution from the hot electrons of the substrate contribute to the XC trace. Because more electrons are excited by the VIS pulse compared to the UV light, the maximum is found at a slightly negative delay of 10 fs.[37]

Because the respective decay times of the solvated electrons are of interest, we focus in the following on the population decay at $t > 0$. To include the finite duration of pump and probe laser pulses, the exponential decay has been convolved with the temporal envelope of pump and probe laser pulses.[37] The dotted lines shown in Figure 4 depict the fitted exponential decay from this analysis. Clearly, the experimental data are reproduced up to 150 fs in the case of D_2O/Ru(001) and up to 300 fs for D_2O/Cu(111). At larger delay, the data deviate significantly from an exponential decay. For D_2O/Ru(001), the determined initial decay time of the solvated electron distribution is $\tau_1^{Ru} = 34(5)$ fs, which is more than four times faster compared to $\tau_1^{Cu} = 140(5)$ fs, found for D_2O/Cu(111).

At later times ($t > 300$ fs) a slowing down of the back transfer compared to the earlier delay is well-discerned in Figure 4. Moreover, the decay of the XC traces for both interfaces becomes comparable to each other. However, to draw quantitative conclusions about the transfer dynamics in this time regime, the time-dependent shift of the e_S peak maximum in the 2PPE spectra toward lower energy (cf. Figure 3) has to be taken into account. An appropriate approach is the comparison of electrons in the identical state of solvation, that is, electrons that have gained the same energy after their photoinjection to the ice CB at time zero. Taking this into account, the time window 280−480 fs for D_2O/Ru(001) corresponds to a time window of 600−800 fs for D_2O/Cu(111), because in both cases, the peak maximum of e_S shifted 0.25(5) eV closer to E_F. Fitting a second exponential decay (dashed lines) to the XC traces within this later time interval leads to transfer times $\tau_2^{Ru} = 302(20)$ fs and $\tau_2^{Cu} = 316(20)$ fs, which are for both interfaces identical within experimental accuracy.

From this simple data analysis we conclude that the population decay of the solvated electrons must be separated into two regimes: (a) at short time delays ($t < 300$ fs), where the XC traces follow an exponential decay with significantly different time constants τ_1 for the two metal substrates and (b) larger time delays ($t > 300$ fs), where the respective transfer rates of D_2O/Ru(001) and Cu(111) are identical. The back transfer in these two regimes is dominated by different properties. Hence, we will discuss the driving mechanisms of back transfer in the limits (a) and (b) separately.

(a) Early Time Delays ($t < 300$ fs): Here the decay time τ_1 for solvated electrons depends on the metal substrate as in D_2O/Ru(001) the decay is four times faster than for D_2O/Cu(111) (Figure 4). At a first glance, this finding can be attributed to different electronic band structures of the metal surfaces. Accordingly, as mentioned in the Introduction, we term this regime of back transfer *substrate-dominated* coupling. Supposing that the ice adlayers are identical on different substrates, the interaction strength depends on the density of the unoccupied states of the metal substrate.[1] To explain our observation of an initial back transfer of solvated electrons for D_2O/Ru(001) to be four times faster than on Cu(111), the density of states (DOS) of the copper substrate should be significantly lower than that of the Ru(001) surface. Figure 5 shows the DOS of Cu and Ru. At the energies of the solvated electrons (hatched area), the DOS of both metals are comparable. Therefore, elastic electron transfer as an origin of the different transfer rates can be excluded on the basis of the DOS. However, the DOS of ruthenium[38] exhibits a prominent maximum 1 eV above E_F as a result of unoccupied d-bands, which lead to a surface resonance at Ru(001).[34] The Cu DOS, on the other hand, is constant in this interval. Considering that this pronounced difference in the unoccupied electronic structure of both

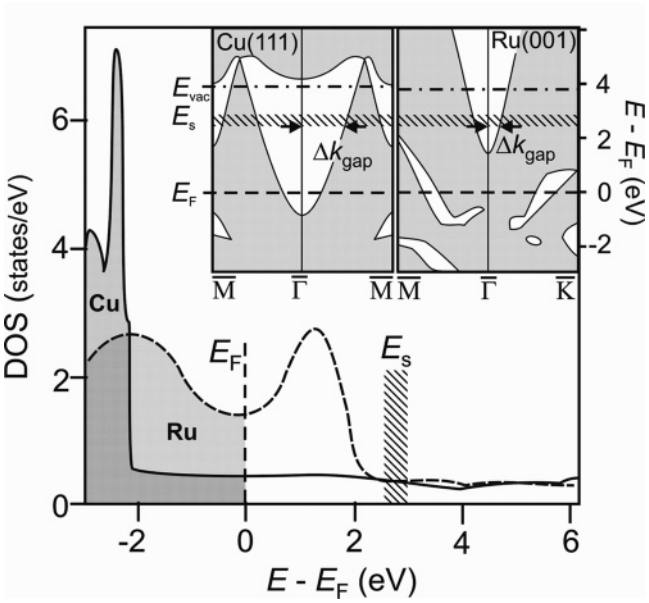

Figure 5. DOS of bulk ruthenium[34] (dashed line) and bulk copper[38] (solid line). Inset: schematic surface band structure of Cu(111) (left) and Ru(001) (right), based on refs 34, 48, and 49. The vacuum levels E_{vac} (dash−dotted lines) refer to the work functions of the metal surfaces covered with an amorphous multilayer D_2O. The energetic distribution, e_S, is indicated by the hatched area.

substrates occurs more than 1 eV below the energy of the solvated electrons at 2.4−2.9 eV above E_F, *inelastic* scattering events should be responsible for the different rates of electron back transfer at the two investigated interfaces. The observed faster back transfer on D_2O/Ru(001) compared to D_2O/Cu(111) thus agrees qualitatively with this conclusion, because the larger phase space for scattering events stemming from the surface resonance on Ru(001) leads to an increase in the inelastic decay probability for the D_2O/Ru(001) interface.[39]

By including details of the electronic structure of the single-crystal substrates projected onto the surface (Figure 5, inset), another difference in the electronic structure, which is relevant for *elastic* electron back transfer, becomes obvious. Both substrates present an orientational band gap in the center of the surface Brillouin zone. However, the width and the bottom of the band gap are substantially different for Cu(111) and Ru(001). The required change in electron momentum, Δk_{gap} (cf. solid arrows in Figure 5), required for elastic electron transfer to the substrate, is larger for Cu(111) compared to that of Ru(001). Because the solvated electrons are localized in real space, they present a wave packet of spatial width Δx and exhibit, as a result of Heisenberg's uncertainty principle, a finite bandwidth in momentum space Δp, as discussed previously.[13,40,41] As pointed out by Borisov et al.,[19] the elastic transfer of a localized electron in front of a metal surface with a momentum spread parallel to the surface is determined by the width of the substrate's band gap in momentum space, Δk_{gap}, at the energy of the respective electronic state. Transitions near $k_{||} = 0$ are prohibited because of the absence of available states in the substrate, and thus, transfer occurs only for $k_{||} > \Delta k_{gap}$. Because for Cu(111) the required momentum transfer Δk_{gap} is larger compared to Ru(001), the observation of a faster initial decay for D_2O/Ru(001) compared to Cu(111) suggests that both elastic and inelastic transfer processes contribute to the electron transfer to the metal. The magnitude of each contribution depends on the details of the electronic structure and the screened Coulomb interaction.

(b) Later Time Delays (t < 300 fs): In this time regime, we observe nearly identical transfer times τ_2 across both interfaces, which are both larger compared to the initial dynamics. We have shown previously[13] that in parallel with energetic stabilization, the localized electronic wave function is constricted further, which leads to a decrease of the wave function overlap with the substrate and consequently to a reduction of the transfer rate. Because the stabilization, which starts from the bottom of the CB (Figure 3), occurs by formation of a solvation shell around the localized electron, a potential barrier evolves simultaneously with the electron solvation process. Regarding the electron back transfer, the height of the barrier between the solvated electron and the metal substrate is determining the transfer rate. According to our observations, the influence of the respective substrate electronic surface band structure becomes less important with increasing delay, because we find that the transfer times τ_2 determined at delays later than 300 fs are comparable for both interfaces. Therefore, we conclude that τ_2 is determined by the tunneling barrier between the solvated electron and the metal surface. This later regime corresponds to the second limit of electron transfer discussed in the Introduction (Figure 1c), where the tunneling probability through the barrier becomes the rate-limiting step. Hence, we refer to this transfer regime (t > 300 fs) as originating from *barrier-determined coupling*.

Summarizing this discussion, we conclude that by comparison of the population decay of solvated electrons in amorphous ice layers on two different metal surfaces we identify two regimes of electron transfer. The initial one is determined by (a) the band structure of the substrate and the wave function overlap with the molecular state, which leads to transfer by elastic and inelastic decay. After several 100 fs, the second regime takes over and (b) the potential barrier between the localized electron and the substrate determines the transfer rate. Both these regimes are illustrated by Figure 6a and b, respectively. As long as the electronic wave function of the solvated electron has significant overlap with metal states and the corrugation of the potential in real space is weak (Figure 6a), the transfer rate is determined by the efficiency of coupling to the substrate states regarding restrictions by momentum and energy conservation. On the other hand, if the barrier is sufficiently high and wide, the tunneling probability through the potential barrier between solvated electron and the substrate (Figure 6b) becomes the rate-limiting step. The separation of these two regimes in a single time-resolved experiment, as presented here, is facilitated by the dynamical evolution of the localization degree of the solvated electron and of the resulting potential barrier.

Before we continue in the next section with an empirical model description of the electron dynamics that combines the competing relaxation processes of electron transfer and stabilization in the ice, we address the energy dependence of the transfer rate, $\tau(E)$. Considering the transfer of solvated electrons, which is determined by tunneling through the barrier, we have to include not only the dynamical evolution of the barrier, but also the simultaneous increase in binding energy. Therefore, we analyze the data by an energy-dependent transfer time, $\tau(E)$, which leads to a weighting of the electron distribution in favor of electrons at low energies. Note that this questions the identification of the peak maximum with the binding energy due to transient changes in the line shape. We will argue that the experimentally determined peak shift per unit time, Σ_S, represents an effective shift of the peak maximum, which has contributions from (i) the energetic stabilization due to rearrangements of the water dipoles proceeding at a rate σ_S and (ii)

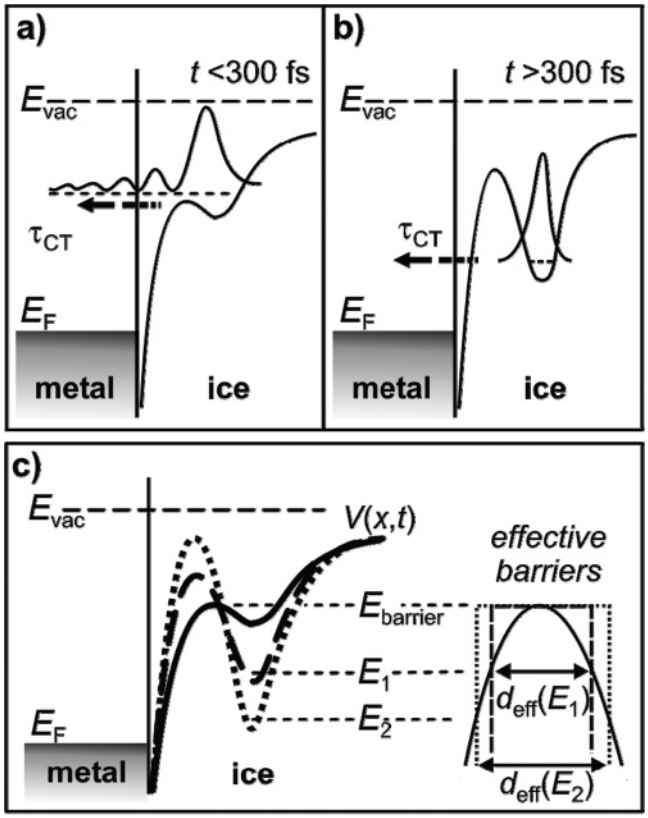

Figure 6. Illustration of electron transfer at ice−metal interfaces. In (a,b) the image potential at the interface, a local corrugation of the potential originating from an attractive site for electron localization, and the corresponding wave function are shown for the two transfer regimes discussed in the text. (a) Substrate-dominated coupling and (b) barrier-determined coupling. In (c), the dynamic evolution of the potential barrier is sketched and parameterized by a series of effective rectangular barriers that describe the tunneling probability through the real barrier.

a shift of the peak maximum due to an energy dependence in the transfer time $\tau(E)$. The latter process leads to a faster decay of energetically higher lying solvated electrons.

Empirical Model Description and Discussion

In this section we introduce an empirical model for electron solvation and transfer dynamics, which, despite its simplicity, reproduces the above data quantitatively and incorporates the competition of electron transfer and energetic stabilization.

Let $N(t,E)$ denote the solvated electron distribution at the time t after photoinjection. The number of electrons at the energy E will (i) *decrease* as a result of back transfer at a rate $\tau^{-1}(E)$ and as a result of the stabilization within the ice layer, which transfers electron population to lower energies, $E - \delta E$, at a constant stabilization rate σ_S. The number of electrons (ii) *increases* as a result of a stabilization of electrons from higher energies, $E + \delta E$, which experience a back transfer rate $\tau^{-1}(E + \delta E)$. The overall change in the population of localized electrons in the adlayer with time delay is assigned to the rate equation

$$\frac{\partial N(t,E)}{\partial t} = \underbrace{-\left(\sigma_s + \frac{1}{\tau(E)}\right)\cdot N(t,E)}_{i} + \underbrace{\left(\sigma_s - \frac{1}{\tau(E+\delta E)}\right)\cdot N(t,E+\delta E)}_{ii} \qquad (1)$$

where the first term (i) describes the population decay and the second one (ii) denotes the population increase. To account for the inhomogeneous distribution of solvation sites within the amorphous ice layer (Figure 2), we used an initial Gaussian energy distribution of solvated electrons with a width of 80 meV at $E - E_F = 2.8$ and 2.9 eV for D_2O on Ru(001) and Cu(111), respectively. To model the transfer in the substrate-dominated regime (Figure 6a), the transfer time was assumed to be constant at $\tau = \tau_0$ for $E > E_{barrier}$. Below $E_{barrier}$, the transfer time becomes energy-dependent $\tau = \tau(E)$ (Figure 6b) due to the dynamic evolution of the barrier during the molecular rearrangement, electron solvation, and screening from the metal substrate. Simultaneously, the crossover from the substrate-dominated to the barrier-determined coupling proceeds. Because neither the shape nor the time-dependence of the barrier is known in detail, we use effective barriers for simplicity. The transmission probability through a rectangular barrier is given by

$$\tau(E)^{-1} = \tau_0^{-1} \exp\left(-\frac{2d}{\hbar}\sqrt{2m(E_{barrier} - E)}\right) \qquad (2)$$

where d denotes the barrier width, m denotes the electron mass, and $E_{barrier}$ denotes the height of the barrier.[42] In our approximation, the rather complex evolution of the real barrier that becomes broader and higher with proceeding solvation (Figure 6c, left) is reduced to effective rectangular barriers. They have a constant height $E_{barrier}$ and an energy-dependent width $d_{eff}(E)$ that accounts for the dependence of the transfer rate on the specific state of solvation. Note that an additional, explicit, time-dependence of d_{eff} is not required to reproduce the experimental data. As a first attempt, we assume d_{eff} to increase like the width of a parabola as illustrated by Figure 6c (right):

$$d_{eff}(E) = \gamma\left(\frac{\hbar}{2}\right)\sqrt{\frac{E_{barrier} - E}{2m}} \qquad (3)$$

where γ is a scaling factor that influences the curvature of the parabola. Using this expression of d_{eff} for the thickness d in eq 2 leads to

$$\tau(E) = \begin{cases} \tau_0 \text{ for } E_{barrier} > E \\ \tau_0 \exp(\gamma(E_{barrier} - E)) \text{ for } E \le E_{barrier} \end{cases} \qquad (4)$$

which means that the transfer times decrease for $E \le E_{barrier}$ exponentially with the electron's binding energy. This is a reasonable outcome that can be ascribed to our choice of the energy-dependence of the barrier widths in eq 3 and justifies the above simplification in d_{eff}.

To simulate our data, the population decay calculated by this model was convolved with the respective temporal laser pulse envelope. The results are represented by the solid lines in Figure 4.[43] Using $E_{barrier} = 2.77$ eV (D_2O/Ru) and 2.93 eV (D_2O/Cu), the model calculations reproduce the population dynamics; the two regimes of back transfer (a) and (b) are simulated in an excellent manner if initial transfer times $\tau_0^{Ru} = 20$ fs and $\tau_0^{Cu} = 67$ fs are chosen. According to eq 4, these time constants reflect the back-relaxation probability before the dynamically evolving tunneling barrier lowers the transfer rate.[44]

We also extracted the time-dependent center of the solvated electron distribution (weighted average or first moment) from the model calculations. For both interfaces, they coincide with the experimental results, as shown in Figure 3 by the solid lines. As a first approximation the energetic stabilization rate σ_S was implemented according to the Holstein model, which assumes a linear variation of the electronic energy as a function of lattice distortion, see eq 1.[45,46] To achieve a simultaneous agreement in the population dynamics (Figure 4) and in the transient peak shift (Figure 3), similar σ_S for the two interfaces were used:

$\sigma_S^{Ru} = 0.24$ eV/ps and $\sigma_S^{Cu} = 0.22$ eV/ps. The coincidence of the experimental data and the simple theoretical description implies an energy gain that is in the investigated delay range independent of the energy of the starting level and progresses linearly with time delay. To understand this agreement, the distinction between the stabilization rate σ_S and the observed transient peak shift $\sum_S(t)$, made in the previous section, becomes important. Only if the nearly equal stabilization rates σ_S^{Ru} and σ_S^{Cu} are used, it is possible to reproduce the experimental data for transfer and peak shift in parallel. Because the peak shift for D_2O/Ru(001) compared to D_2O/Cu(111) is three times faster, the model corroborates that the observed change in the energy of the peak maximum of the solvated electron distribution, denoted by $\sum_S(t)$, is not identical with the real energetic stabilization σ_S of the solvated electrons. It represents, in fact, a combination of stabilization and energy-dependent back transfer. Moreover, the agreement of the two stabilization rates σ_S^{Ru} and σ_S^{Cu} suggests that the local environment of the solvated electron, that is, the solvation shell, differs only slightly for the two employed substrates.

The parameter γ in eq 3 is a measure of the relation between the effective barrier thickness at the interfaces at a fixed $\Delta E = E_{barrier} - E$. In the simulation, γ^{Ru} was chosen to be twice as large as γ^{Cu}, that is, the barrier for D_2O/Ru(001) is effectively twice as wide as for D_2O/Cu(111).[47] This is a reasonable assumption, because for a single BL coverage of D_2O/Ru(001), no indication for electron solvation is found (data not shown). As discussed before, D_2O forms a well-ordered first BL on Ru(001) as a result of the stronger adsorbate−substrate interaction before the amorphous multilayer evolves on top of it. In contrast, amorphous ice on Cu(111) forms islands for single BL coverage as a result of the weaker ice−metal interaction, which might well result in a difference in the interfacial electronic structure for the two investigated interfaces. Considering that $\gamma^{Cu} \approx 2\gamma^{Ru}$, we suggest that for D_2O/Ru(001) the well-ordered first BL acts as a spacer layer that is inactive for electron solvation and keeps the solvated electron further away from the interface.

To summarize this section, we note that a simple rate equation model reproduces nicely our time-resolved 2PPE data. This is noteworthy because the tunneling barrier description used in the calculation simplifies the complex evolution of the real potential barrier to effective rectangular barriers. Furthermore, the model calculation emphasizes that the shift in energy of the solvated electron peak maximum $\sum_S(t)$ cannot be identified with the energetic stabilization of the electron. It rather represents the association and competition of back transfer and stabilization dynamics.

Conclusions

Using femtosecond time-resolved two-photon photoelectron spectroscopy, we have studied electron-transfer dynamics at interfaces of amorphous ice layers and single-crystal metal electrodes as a model system for heterogeneous electron transfer. The study facilitates insight into the microscopic processes taking part in electron transfer. Electrons are photoinjected from the metal substrate into the ultrathin ice layer where they localize and form solvated electrons. As a result of the subsequent dynamical evolution of the molecular environment, a solvation shell and a potential barrier surrounding the electron, which decouples the electron from the metal, is formed. With progressing delay, the solvated electrons increase their degree of confinement and are screened from the metal during the first few hundred femtoseconds. Comparing the dynamics at the two interfaces of D_2O on Cu(111) and on Ru(001), we observe a dynamical crossover between two limits of electron transfer. These limits are (i) transfer from a weakly localized state in the ice layer to the metal and (ii) transfer of a strongly confined electron wave packet, which represents the solvated electron, by tunneling through a potential barrier. These two regimes have been identified by an analysis of the dynamics in population and binding energy from experimental data and, additionally, by use of an empirical model description. During the first few 100 fs different transfer times τ_1 are determined for the two interfaces ($\tau_1 = 34$ fs for Ru; $\tau_1 = 140$ fs for Cu). After 300 fs, the transfer times increase ($\tau_2 > \tau_1$) and agree within the experimental accuracy for both interfaces ($\tau_2 = 302$ fs for Ru; $\tau_2 = 316$ fs for Cu). We conclude that in the early time interval the different electronic structures of the metal electrodes are responsible for variations in τ_1. The faster transfer at the D_2O/Ru(001) interface compared to the Cu(111) case is consistent with elastic and inelastic transfer processes, which are governed by details of the electronic structure of the metal substrate. The fact that τ_1 differs for both interfaces emphasizes that the transfer times are determined by the electronic structure of the substrate, which requires a considerable overlap of the electron injected into the ice layer. This process is, thus, similar to the decay of a state with an extended wave function, like an IPS. During the later regime, when the transfer times τ_2 are identical, the substrate plays a minor role in the transfer process. This crossover is explained by a dynamical formation of a potential barrier, which confines the solvated electron and screens it from the metal. Apparently, the solvation shell and, thus, the potential barrier is independent of the selected substrate, which suggests a general relevance of our conclusions. Our study demonstrates nicely that the degree of electron confinement, which is determined by the configuration change of the molecular environment upon injection of an excess charge, is important for microscopic insight in electron-transfer processes at interfaces.

Acknowledgment. We thank A. Rubio for fruitful discussions and gratefully acknowledge funding by the Deutsche Forschungsgemeinschaft through SPP 1093 and by the German-Israeli-Foundation through GIF 777.

References and Notes

(1) Zhu, X.-Y. *J. Phys. Chem. B* **2004**, *108*, 8778.
(2) Miller, R. J. D.; McLendon, G. L.; Nozik, A. J.; Schmickler, W.; Willig, F.; *Surface Electron-Transfer Processes*; VCH: New York, 1995.
(3) Adams, D. M.; Brus, L.; Chidsey, C. E. D.; Creager, S.; Creutz, C.; Kagan, C. R.; Karnat, P. V.; Lieberman, M.; Lindsay, S.; Marcus, R. A.; Metzger, R. M.; Michel-Beyerle, M. E.; Miller, J. R.; Newton, M. D.; Rolison, D. R.; Sankey, O.; Schanze, K. S.; Yardley, J.; Zhu, X. *J. Phys. Chem. B* **2003**, *107*, 6668.
(4) Nitzan, A.; Ratner, M. A. *Science* **2003**, *300*, 1384.
(5) Pope, M.; Swenberg, C. E. *Electronic Processes in Organic Crystals and Polymers*; Oxford University Press: Oxford, 1999.
(6) Migus, A.; Gauduel, Y.; Martin, J. L.; Antonetti, A. *Phys. Rev. Lett.* **1987**, *58*, 1559.
(7) Pépin, C.; Goulet, T.; Houde, D.; Jay-Gerin, J.-P. *J. Phys. Chem. A* **1997**, *101*, 4351.
(8) Hertwig, A.; Hippler, H.; Unterreiner, A.-N. *Phys. Chem. Chem. Phys.* **2002**, *4*, 4412.
(9) Paik, D. H.; Lee, I.-R.; Yang, D.-S.; Baskin, J. S.; Zewail, A. H. *Science* **2004**, *306*, 672.
(10) Turi, L.; Sheu, W.-S.; Rossky, P. J. *Science* **2005**, *309*, 914.
(11) Verlet, J. R. R.; Bragg, A. E.; Kammrath, A.; Cheshnovsky, O.; Neumark, D. M. *Science* **2005**, *307*, 93.
(12) Gahl, C.; Bovensiepen, U.; Frischkorn, C.; Wolf, M. *Phys. Rev. Lett.* **2002**, *89*, 107402.
(13) Bovensiepen, U.; Gahl, C.; Wolf, M. *J. Phys. Chem. B* **2003**, *107*, 8706.
(14) Bovensiepen, U. *Prog. Surf. Sci.* **2005**, *78*, 87.
(15) Gahl, C. Ph.D. Thesis, Freie Universität Berlin, Germany, 2004, http://www.diss.fu-berlin.de/2004/338/.

(16) McNeill, J. D.; Lingle, R. L., Jr.; Ge, N.-H.; Weng, C. M.; Jordan, R. E.; Harris, C. B. *Phys. Rev. Lett.* **1997**, *79*, 4645.
(17) Marinica, D. C.; Ramseyer, C.; Borisov, A. G.; Teillet-Billy, D.; Gauyacq, J. P.; Berthold, W.; Feulner, P.; Höfer, U. *Phys. Rev. Lett.* **1997**, *79*, 4645.
(18) Echenique, P. M.; Berndt, R.; Chulkov, E. V.; Fauster, Th.; Goldmann, A.; Höfer, U. *Surf. Sci. Rep.* **2004**, *52*, 219.
(19) Borisov, A. G.; Gauyacq, J. P.; Kazansky, A. K.; Chulkov, E. V.; Silkin, V. M.; Echenique, P. M. *Phys. Rev. Lett.* **2001**, *86*, 488.
(20) Gadzuk, J. W. *Surf. Sci.* **1995**, *342*, 345.
(21) Knoesel, E.; Hotzel, A.; Wolf, M. *Phys. Rev. B: Condens. Matter* **1998**, *57*, 12812.
(22) Funk, S.; Bonn, M.; Denzler, D. N.; Hess, Ch.; Wolf, M.; Ertl, G. *J. Chem. Phys.* **2000**, *112*, 9888.
(23) Schmitz, P. J.; Polta, J. A.; Chang, S. L.; Thiel, P. A. *Surf. Sci.* **1987**, *186*, 219.
(24) Held, G.; Menzel, D. *Surf. Sci.* **1995**, *327*, 301.
(25) Bovensiepen, U.; Gahl, C.; Stähler, J.; Wolf, M. *Surf. Sci.* **2005**, *584*, 90.
(26) Smith, R. S.; Kay, B. D. *Surf. Rev. Lett.* **1997**, *4*, 781.
(27) Henderson, M. A. *Surf. Sci. Rep.* **2002**, *46*, 1.
(28) Gahl, C.; Bovensiepen, U.; Frischkorn, C.; Morgenstern, K.; Rieder, K.-H.; Wolf, M. *Surf. Sci.* **2003**, *532*−*535*, 108.
(29) Denzler, D. N.; Hess, Ch.; Dudek, R.; Wagner, S.; Frischkorn, Ch.; Wolf, M.; Ertl, G. *Chem. Phys. Lett.* **2003**, *376*, 618.
(30) Feibelman, P. J. *Science* **2002**, *295*, 99.
(31) Andersson, K.; Nikitin, A.; Pettersson, L. G. M.; Nilsson. A.; Ogasawara, H. *Phys. Rev. Lett.* **2004**, *93*, 196101.
(32) Weissenrieder, J.; Mikkelsen, A.; Andersen, J. N.; Feibelman, P. J.; Held, G. *Phys. Rev. Lett.* **2004**, *93*, 196102.
(33) For D_2O/Ru(001), the maximum of e_S at zero time delay occurs 100 meV lower in energy due to a lower work function of $\Phi = 3.9$ eV compared to 4.0 eV for D_2O/Cu(111).
(34) Seitsonen, A. P. Ph.D. Thesis, Technical University Berlin, Berlin, Germany, 2000, http://edocs.tu-berlin.de/diss/2000/seitsonen_ari.htm.
(35) Note that this statement still holds if one would correct for the different initial energies of 100 meV at zero time delay.
(36) Hertel, T.; Knoesel, E.; Wolf, M.; Ertl, G. *Phys. Rev. Lett.* **1996**, *76*, 535.
(37) Time zero is determined independently. An autocorrelation function of pump and probe laser pulses is fitted to the time-dependent 2PPE intensity at $E - E_F > 3.5$ eV. The temporal envelope of the laser pulses is taken as a sech^2. The pulse duration is determined by this analysis to 27(5) fs and 57(5) fs for D_2O/Ru(001) and D_2O/Cu(111), respectively.
(38) Papaconstantopoulos, D. A. *Handbook of the Band Structure of Elemental Solids*; Plenum Press: New York, 1986.
(39) Echenique, P. M.; Pitarke, J. M.; Chulkov, E. V.; Rubio, A. *Chem. Phys.* **2000**, *251*, 1.
(40) Andrianov, I.; Klamroth, T.; Saalfrank, P.; Bovensiepen, U.; Gahl, C.; Wolf, M. *J. Chem. Phys.* **2005**, *122*, 234710.
(41) Szymanski, P.; Garrett-Roe, S.; Harris, C. B. *Prog. Surf. Sci.* **2005**, *78* 1.
(42) Schwabl, F. *Quantum Mechanics*; Springer, Berlin, 1992.
(43) A further single-exponential decay to negative delays was added to account for hot electrons in the metal.
(44) Note that the energy-dependent transfer times $\tau(E)$ cannot simply be set equal with the rate constants τ_1 and τ_2 mentioned in the previous section. The data shown in Figure 4 is the *integrated* 2PPE intensity within 2.4 and 2.8 (2.9) eV in the case of the Ru(001) and the Cu(111) substrates, respectively. To fit the data, this integration was also done in the model calculation.
(45) Harris, C. B.; Ge, N.-H.; Lingle, R. L., Jr.; McNeill, J. D.; Wong, C. M. *Annu. Rev. Phys. Chem.* **1997**, *48*, 711.
(46) Emin, D.; Holstein, T. *Phys. Rev. Lett.* **1976**, *36*, 323.
(47) Indeed the extracted effective widths are in the order of several angstrœms: $d_{\mathrm{eff}}^{\mathrm{Cu}}(0.1\ \mathrm{eV}) = 1.8$ Å, $d_{\mathrm{eff}}^{\mathrm{Ru}}(0.1\ \mathrm{eV}) = 3.6$ Å, $d_{\mathrm{eff}}^{\mathrm{Cu}}(0.3\ \mathrm{eV}) = 3.2$ Å, and $d_{\mathrm{eff}}^{\mathrm{Ru}}(0.1\ \mathrm{eV}) = 6.4$ Å. But these values are *not* to be set equal with the exact distance of the solvated electron from the metal surface in the respective state of solvation.
(48) Smith, N. V. *Phys. Rev. B: Condens. Matter* **1985**, *32*, 3549.